Visual Abstract

Web post-buckling strength of thin-webbed cellular beams using carbon PFRP profiles

Hamda Guedaoura, Yazid Hadidane
Civil Engineering Laboratory, Badji Mokhtar- Annaba University, P. O. Box 12, 23000 Annaba, Algeria
hamda.guedaoura@gmail.com; hamda.guedaoura@univ-annaba.org
y.hadidane@gmail.com; yazid.hadidane@univ-annaba.dz

ABSTRACT. Currently, cellular steel beams are widely used by structural engineers and major companies due to their useful structural applications and serviceable performance. However, these types of steel beams are susceptible to different states of instability and failure mechanisms such as web post-buckling. The aim of this paper is to investigate the effectiveness of using externally bonded pultruded carbon fiber (CFRP) profiles for the strengthening of web post-buckling in thin webbed cellular beams as an alternative to the typical welding technique of reinforcement. A proposed numerical model created with the finite element software ABAQUS capable of capturing the de-bonding and fracture along the adhesive layer between steel and CFRP has been validated using published experimental results. The suggested numerical model is then used to simulate the parametric analysis of using pultruded CFRP T and U sections to strengthen six cellular beams of various sizes. It was found that this novel technique was able to prevent the web post-buckling failure mode or delay it to a grater load with a considerable strength enhancement comparable to control beams.

KEYWORDS. Cellular beams; Web post-buckling; Pultruded CFRP profiles; Finite element models; Failure modes.

OPEN ACCESS

Citation: Guedaoura, H., Hadidane, Y., Web post-buckling strength of thin-webbed cellular beams using carbon PFRP profiles, Frattura ed Integrità Strutturale, 60 (2022) 43-61.

Received: 18.12.2021
Accepted: 19.01.2022
Online first: 23.01.2022
Published: 01.04.2022

INTRODUCTION

With the high demand of smart home purchases, structural engineers are always striving to achieve better functionality, solidity and aesthetic aspects. Steel beams with web openings for example are the most useful solution to integrate lines and cables through the web penetration without reducing the floor depth in modern steel frame buildings. However compared to the ordinary steel I beams , in some cases, such web openings causes a state of instability and different failure modes, according to several writers [1–5]: Web post buckling, Flexure mechanism, Vierendeel mechanism, Lateral torsional buckling of the beam and welded joint Rupture in the web post are the common failure modes of cellular and castellated beams. Recently comprehensive parametric studies were carried out by Morkhade and al [6,7] to

investigate the load carrying capacity of steel beam with multiple web openings of various sizes and shapes, it was found that the ultimate load of tested beams was sensitive to the openings sizes, positions and geometry.
Different other researches focused on web post instability in cellular beams, Tsavdaridic and D'Mello [8] investigated buckling behavior of web-post between two adjacent web openings in cellular beam, Panedpojaman et al [9]conducted numerical parametric study to investigate the web-post buckling of cellular beams and proposed design equations to assess the local shear strength in web posts. In the same axis, a new analytical formulation was proposed by Grilo and al [10] to assess the shear resistance of web post buckling in cellular beams. So an appropriate strengthening method was required to maintain and preserve the stability of the web post portion and increase the strength of cellular beams after usage, change of the design rules, or augmentation in live loads.
Till date, the only strengthening technique of cellular beams in most published investigations and design guidelines is the welding of steel stiffeners in the instability region or around the apertures based on Darwin Approach [11] or Hicks and Lawson Approach [12]. Despite the fact that the effectiveness of this strengthening technique has been confirmed in various studies [13,14], repaired sections are sensitive to fatigue problems due to residual stresses and strains produced by welding operation as well as corrosion vulnerability and practical difficulties during installation are all drawbacks of welding technique which cannot be overlooked, This was the motivation that drove engineers and researchers to find an alternative method for strengthening steel structures.
Due to their Superior properties CFRP and GFRP products are more attractive than other composite materials of strengthening, they can be used in form of pultruded profiles, plates or sheets. Using three strengthening technique Zhao and al [15] investigated the CFRP plate strengthening of web buckling in 21 steel beams, according to the strengthening method distinct increases in the ultimate load was found in comparison to control beams, the third configuration "C" which employed CFRP on both sides of the web showed the highest increases from 250% to 500% in ultimate load (Fig.1). Narmaashiri and al [16] tested eight steel I beams strengthened with CFRP plate bonded to the bottom flange, it was observed that ultimate loads and failure modes were influenced by the CFRP plate thickness. In other hand Zeng and al [17] studied the interfacial behavior and debonding failure of full scale H section steel beams reinforced with CFRP plate, it was found that the proposed three dimensional model was able to predict the debonding failure mode and validate their experimental results. Okeil and al [18] used pultruded FRP profiles to prevent web buckling in steel plate girder by bonding GFRP T section as stiffeners (Fig.2). The ultimate load was improved by 40% and 56% for vertical and diagonal configurations, respectively, and the undesirable web buckling was delayed to a higher load, in the same axis this strengthening by stiffening technique (SBS) was extensively studied by Ulger and al [19] and it's efficiency was confirmed.

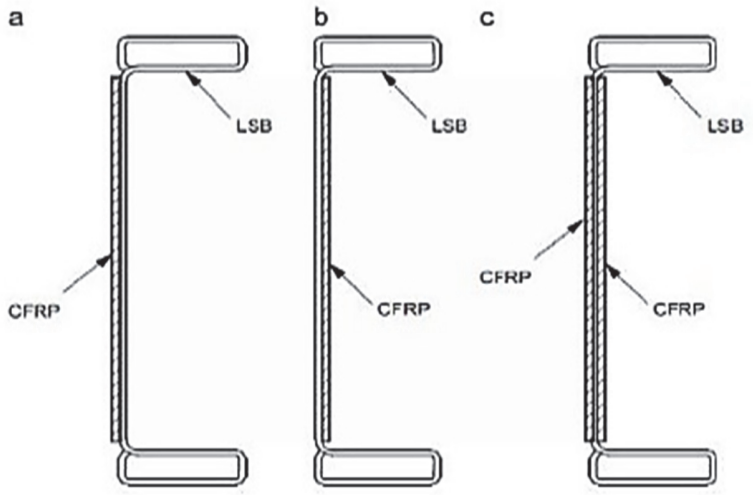

Figure 1: Web strengthening technique used by Zhao et al [15].

To date, no guidance and only a small number of studies on the use of FRP materials to reinforce steel beams having web openings. Numerical and experimental studies were conducted by Altaee and al [20,21] on the strengthening of steel beams with rectangular opening in different positions along the span using HM CFRP plates , it was discovered that using a suitable strengthening system, CFRP was able to recover the strength and stiffness of tested beams. Mustafa and al [22] performed another numerical study employing NM CFRP and BFRP to reinforce steel beams with single circular and rectangular

openings in distinct places under cyclic loads, The strength of the tested beams was restored utilizing the optimal CFRP and BFRP plate thickness and arrangement. Hamood and al [23] conducted an experimental study on seven steel-plated girders subjected to shear loading with square and diamond web perforations and reinforced with two types of CFRP layouts. The ultimate shear force for strengthened specimens was increased by 9 to 21%. The sole research on strengthening castellated beams with CFRP sheet was undertaken by Cyril and Baskar [24], as a result of their tests, the stiffness and flexural capacity of the reinforced specimens were raised differently depending on the CFRP strengthening pattern.

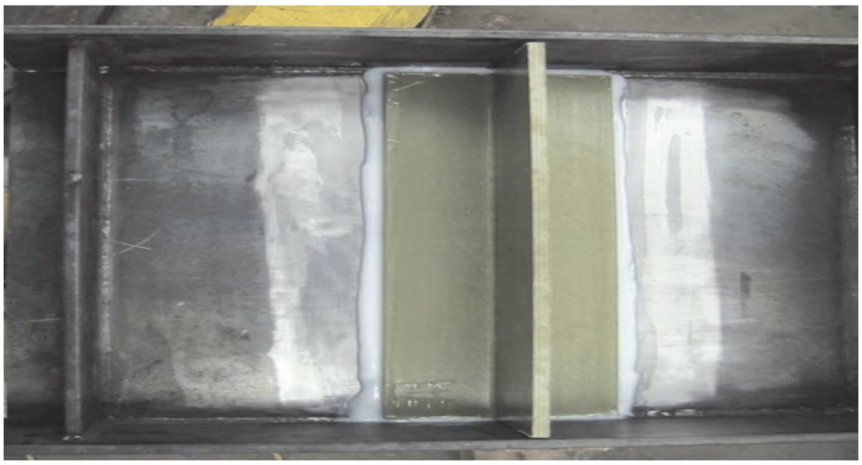

Figure 2: Glass FRP T section stiffening used by Okeil et al. [18].

The few studies that have been done are limited to recover the flexural strength of steel beams after the creation of web openings using FRP plates or sheets, many aspects are yet to be investigated. So in this study, a novel technique on strengthening web post-buckling of cellular beams using pultruded CFRP profiles will be suggested to acquire more sufficient information about the use of FRP laminates to strength steel beams with web openings and achieve an advanced phase in which guidelines and codes can be developed to assist engineers in the design and application of such systems.

NONLINEAR FINITE ELEMENT MODEL

The three-dimensional (3D) finite element (FE) model created in the commercial FE package ABAQUS /CAE [25–28] to simulate the nonlinear analysis of cellular beams with and without CFRP strengthening is described and validated in this part:

Solver type and material modelling

In the first step, an elastic buckling analysis was carried out to determine the web-post failure mode that occurred in the experimental test. Then the "Dynamic, Explicit" provided by (ABAQUS/EXPLICIT) was the suitable solver type used in this study which has been proven to be more efficient for solving quasistatic problems compared to the implicit method which may need a high number of iterations and more additional processing time [29,30]**.** Both material and geometric non-linearity were taken into account in this model to describe the large deformation and local instability effects. A bilinear stress-strain chart without strain hardening was adopted for the steel material [10,31] whereas FRP was treated as orthotropic elastic material until failure [17]. The adhesive was modeled using the bilinear traction-separation law [17,21,30]. The general-purpose shell element S4R with reduced integration was adopted for both steel and FRP, while the adhesive was modeled using the 8-node cohesive element COH3D8 [17,21].

Cohesive

As the cohesive surface approach is not supported in ABAQUS/EXPLICIT solver to model the bond behavior between steel/CFRP the cohesive element approach which can simulate bond behavior from initial loading to damage initiation and propagation has been used in this study [29]. The tie constraint of the cohesive element surfaces to the steel and CFRP is used to achieve that debonding growth occurs along the adhesive layer, without deformation of the adjacent parts.

Damage modelling of adhesive

The damage model that was implemented from the aforementioned approach has two stages: damage initiation and damage evolution [29]:

Among the four damage initiation criteria provided by ABAQUS, the quadratic nominal stress criterion is used in this study, which can be written as:

$$\left(\frac{<t_n>}{\sigma_{max}}\right)^2+\left(\frac{t_s}{\tau_{max}}\right)^2+\left(\frac{t_t}{\tau_{max}}\right)^2=1 \tag{1}$$

A scalar damage variable D is introduced as the total damage in the material after damage initiation. D has a range of 0 to 1, with 0 signifying undamaged and 1 representing total separation, so the corresponding stress components are then degraded as follows [29]:

$$t_n=\begin{cases}(1-D)\overline{t_n} & \overline{t}_n\geq 0\\ \overline{t}_n & \overline{t}_n<0\end{cases} \tag{2}$$

$$t_t=(1-D)\overline{t_t} \tag{3}$$

$$t_s=(1-D)\overline{t_s} \tag{4}$$

The expression of the variable D in ABAQUS which assumes the linear softening of the damage evolution is:

$$D=\frac{\delta_m^f\left(\delta_m^{max}-\delta_m^0\right)}{\delta_m^{max}\left(\delta_m^f-\delta_m^0\right)} \tag{5}$$

Residual stresses and geometric imperfection

Residual stresses are not included in this FE element model in accordance with earlier recommendations [24]. The initial geometric imperfection was introduced in the models with a scale factor of H/500 [9] which was determined to be suitable for all tested beams.

Mesh and boundary conditions

Based on mesh convergence study, mesh size of 20 mm x 20mm for both steel and composite material exhibited satisfactory convergence with corresponding experimental results. Loading and boundary conditions are similar to experimental tests (Figs. 3 and 4). The support conditions of cellular beams were ($U_y=0$, $U_x=0$, $\theta_z=0$) applied at the beam ends besides to that a point was created in the mid span of the top flange to apply ($U_Z=0$, $U_X=0$) to prevent out of plain torsional buckling, the load was applied on the top flange with an eccentricity of 20 mm from the mid-span . For the reinforced beam (B3-R0) The load was applied uniformly to the top flange, and vertical restraint conditions (Uy=0) were applied at the beam ends using the MPC constraint option, which shared the entire cross-section to prevent stress localization, in addition the beam was laterally restrained (Ux=0) along the top flange.

Finite element model validation

As the accuracy of numerical model results depends strongly on the modeling technique, a comparative study will be conducted between the adopted FE model and some of previous available experimental test results. Because of the novel nature of this work and from literature research, it was decided to use experimental test namely Grilo et al [10] to simulate the web post-buckling of unstrengthened cellular beams and the only experimental test conducted by Altaee et al [20] to remodel the web post-buckling strengthening between two adjacent rectangular openings using pultruded CFRP plates of 200 GPa elastic modulus bonded with an adhesive of 1.5 GPa elastic modulus and 29 MPa tensile strength. All dimensions and properties of tested beams are detailed in Figs. 5 and 6, and Tabs. 1 and 2.

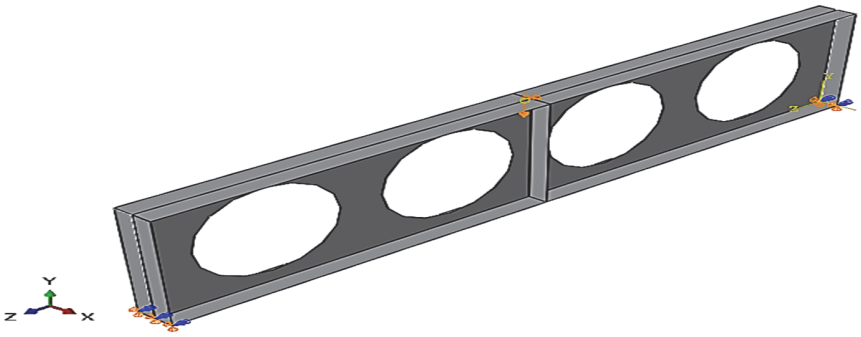

Figure 3: Loading and Boundary conditions used for tested cellular beams.

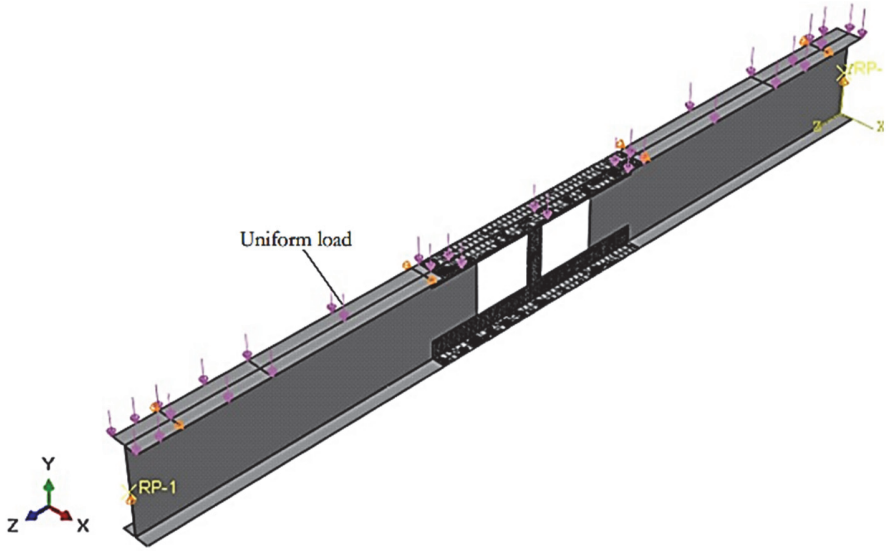

Figure 4: Loading and Boundary conditions of specimen B3-RO.

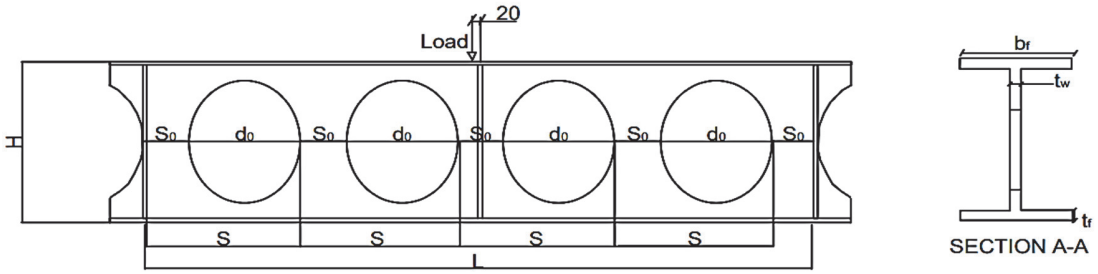

Figure 5: Dimensions and details of tested cellular beams by Grilo and al [17].

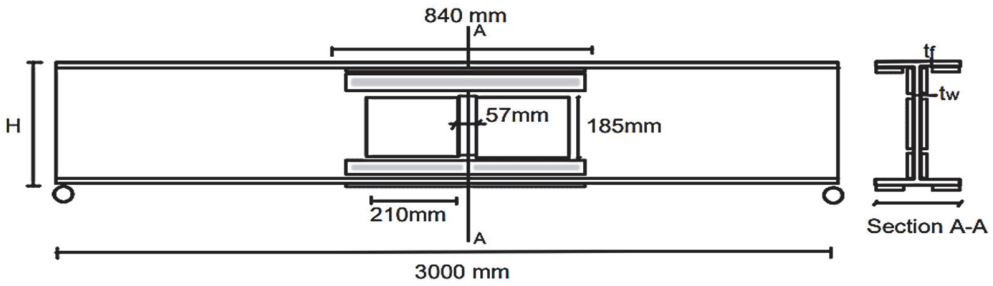

Figure 6: Dimensions and details of specimen B3-RO tested by Altaee and al [20].

Test	Specimen	t_w (mm)	t_f (mm)	b_f (mm)	S (mm)	H (mm)	L (mm)	d_o (mm)	f_y (MPa)	E (GPa)
Grilo and al [10]	A2	4.8	5.6	102	445.8	433	1874	342.5	416	200
	A5	4.6	6	102	325.1	409	1370	248.8	416	200
	B2	5.4	9	101	458.3	440	1933	352.1	365	200
	B5	5.9	9	99	318.4	412	1346	243.8	398	200

Table 1: Details and dimensions of tested cellular beams.

Test	Specimen	t_w (mm)	t_f (mm)	b_f (mm)	H (mm)	L (mm)	*Web* f_y (MPa)	*Flunge* f_y (MPa)	Web E (GPa)	Flunge E (GPa)
Altaee and al [20]	B3-RO	5.8	7	101.6	305.1	3000	435	412	210	206

Table 2: Details and dimensions of specimen B3-RO.

Finite element validation results

Ultimate loads of tested beams obtained from the developed FE model were compared to their corresponding experiment data as detailed in Tab3. It can be seen that ultimate load differences do not exceed 6% for all tested beams, and that load-deflection curves of numerical and experimental results were in good agreement (Fig. 7). The failure modes of all cellular beams in FE models were similar with experimental test results (Tab.3), all specimens failed by web post-buckling as shown in Fig. 8. The specimen "B3-RO" failed by lateral-torsional buckling accompanied by top flange yielding in the experimental test, the same failure mode was also observed in the FE model (Fig. 9). Using the numerical output SDEG (stress degradation parameter) provided by ABAQUS which is equal initially to 0 and evolves monotonically to 1 for the overall damage of bond interface [29], the numerical model was able to predict the bond failure between steel and CFRP, this can also be proven by the adhesive layer deletion (Fig .10). The good level of agreement from these results provides confidence to use the developed numerical model on strengthening web post-buckling of cellular beams using carbon PFRP profiles.

Specimen	P_u (exp) (kN)	P_u (fe) (kN)	Percental difference (%)	Failure mode
A2	123.7	123.82	-0.09	WPB
A5	198.2	209.63	-5.76	WPB
B2	157.9	151.18	4.25	WPB
B5	276.9	290.77	-5.00	WPB
B3-R0	442	442.90	0.00	LTB+TFY+DEB
	Average		-1.32	

Table 3: FE and experimental ultimate load comparison.

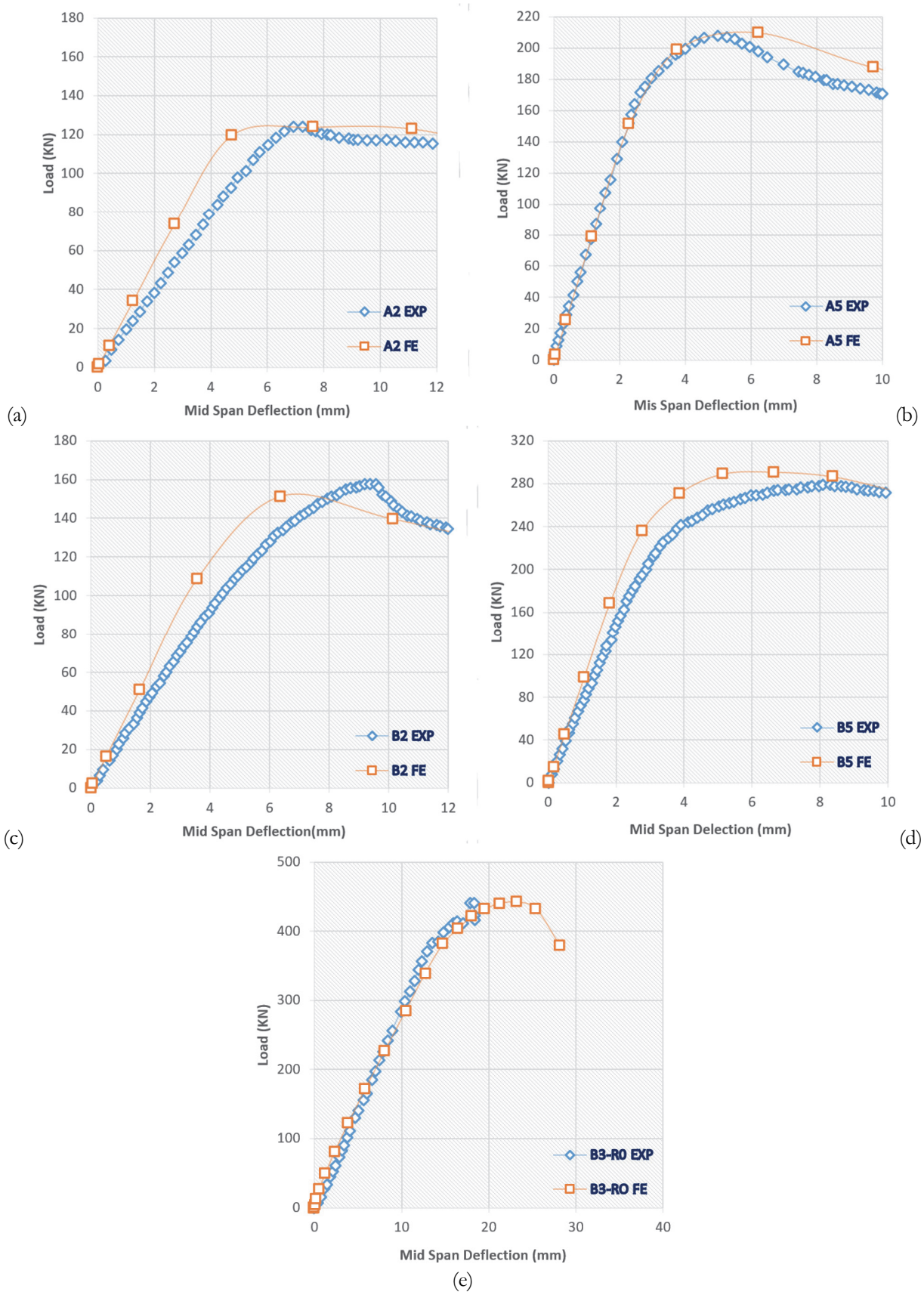

Figure 7 : Load – deflection curves of specimens: a) A2; b) A5; c) B2; d) B5; e) B3-R0.

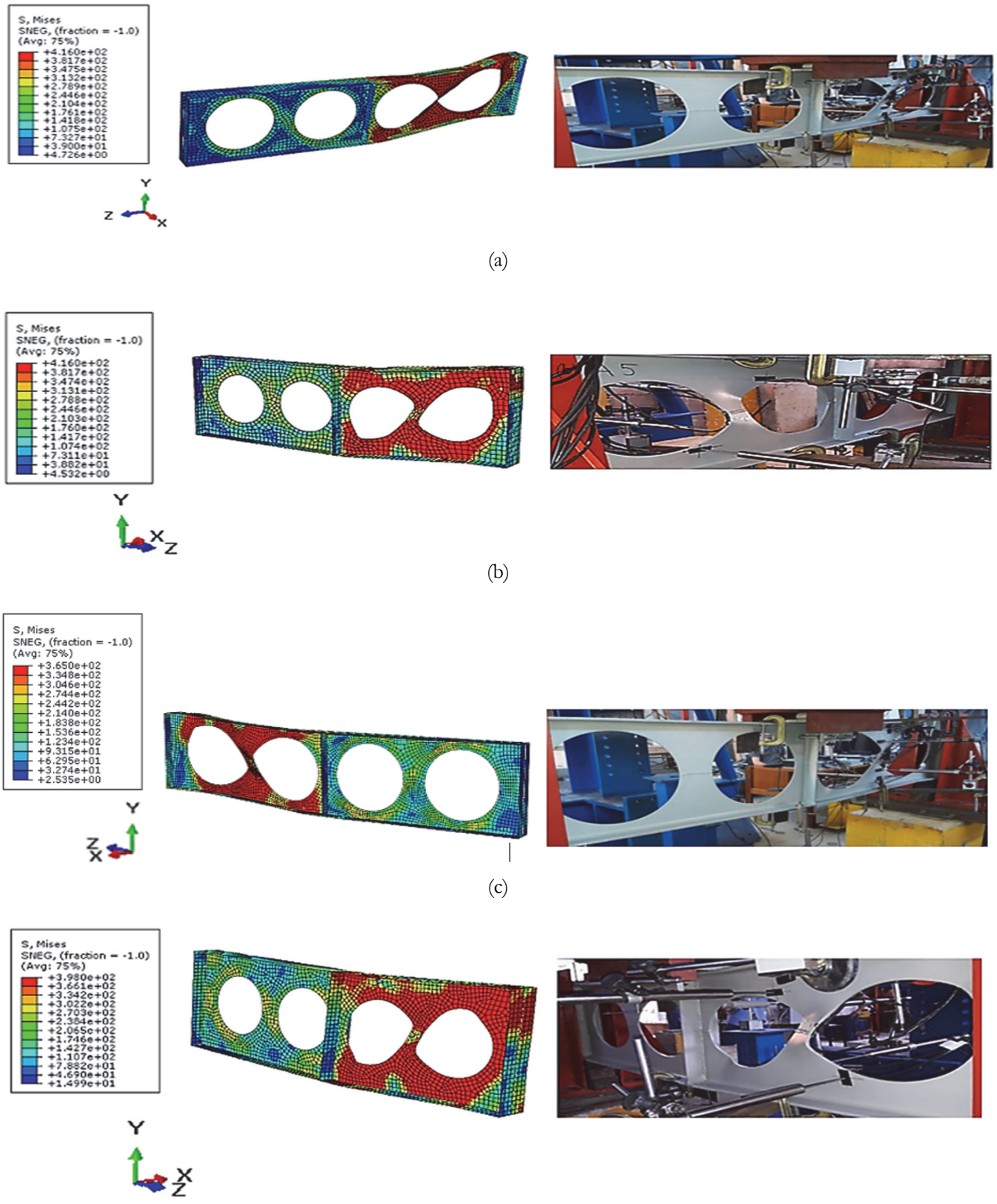

Figure 8: FE and experimental failure mode of cellular beams: a) Specimen A2; b) Specimen A5; c) Specimen B2; d) Specimen B5.

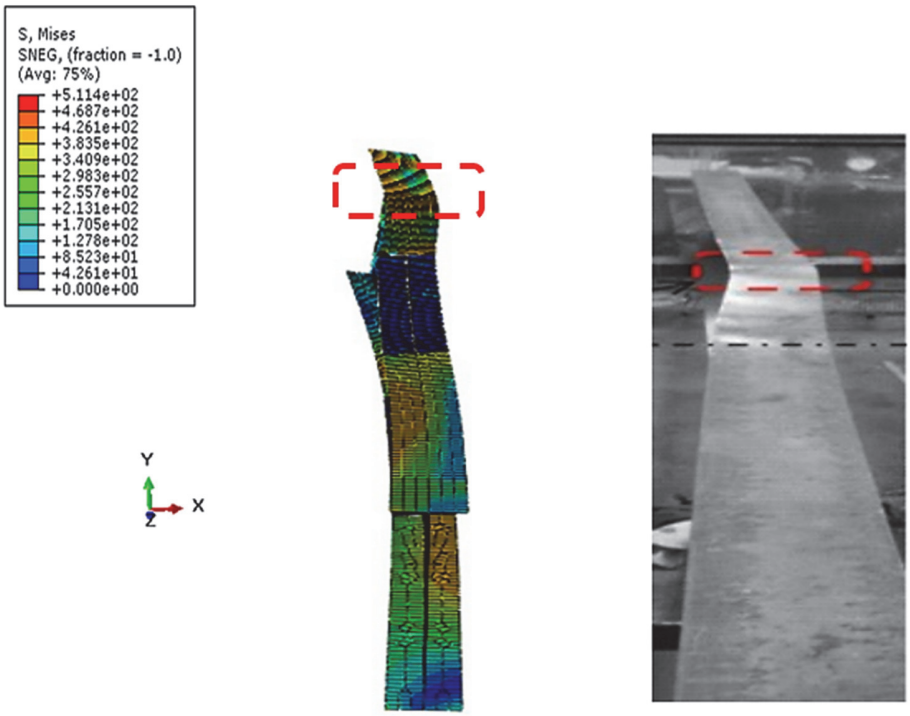

Figure 9: FE and experimental failure mode of specimen B3-RO.

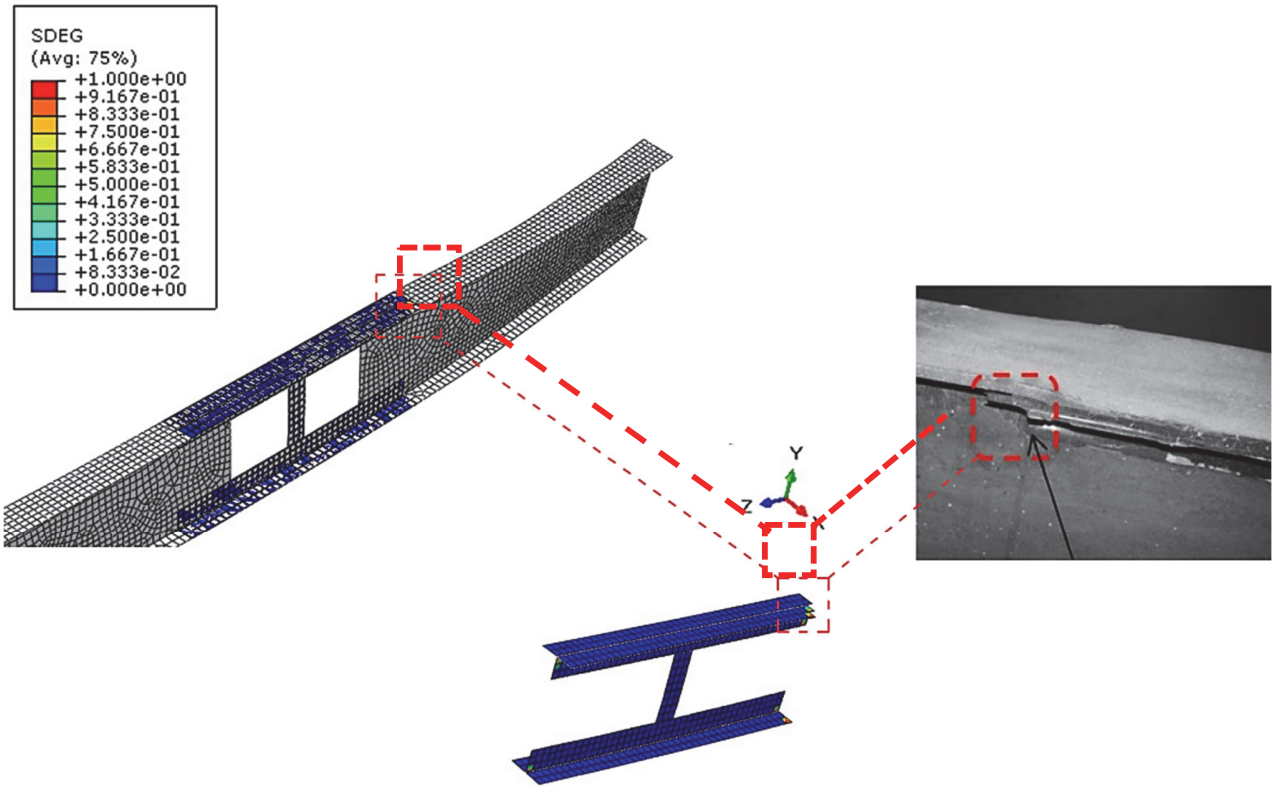

Figure 10: FE and experimental CFRP plate debonding.

CASE STUDY

Model description

The verified cellular beams in the previous section: A2, A5, B2, and B5 were strengthened using two pultruded CFRP profiles sections bonded in the instability region (Fig. 11): The T shaped Section and U section (Fig. 12).

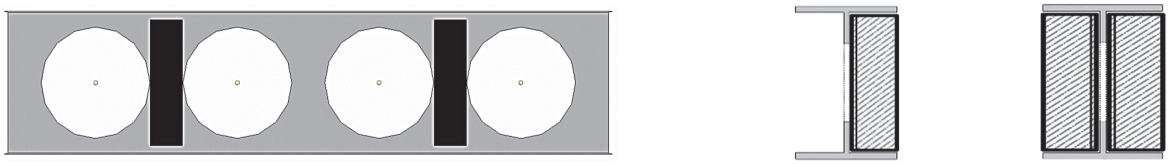

(a) (b)

Figure 11: Strengthening configuration and bonding positions: (a) PS1 configuration and (b) PS2 configuration.

(a) (b)

Figure 12: CFRP pultruded profiles: (a) U section and (b) T section.

As the selection of an optimum CFRP profile dimension for our case is not specified in any design rule, for all tested specimens the pultruded stiffener's width was selected to be equal to the web post width while the length was preferred to cover the full depth of the web post and avoid the weld seam between the web post and the flange for all tested specimens. Tab. 4 and Fig. 13 resume all profile dimensions used for every corresponding specimen.

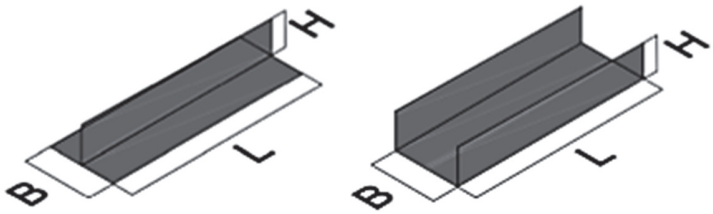

Figure 13: CFRP pultruded profiles dimensions.

Specimens	T section dimensions (mm)			U section dimensions (mm)		
	B	L	H	B	L	H
A2	103	419	50	103	419	50
B2	106	423	50	106	423	50
A5	76	396	50	76	396	50
B5	74	393	50	74	393	50

Table 4: CFRP pultruded profiles dimensions.

The impact of bonding pultruded stiffeners in one side and two opposing sides was investigated in this study using two strengthening configurations named PS1 and PS2 respectively (Fig. 11). The impact of various CFRP profile thicknesses was also considered. The CFRP elastic modulus in the fiber direction was 200 GPa [20], and the adhesive tensile young's modulus was 11.3 GPA with a tensile strength of 22.3 MPa [17]. The effect of web post slenderness on the strengthening technique was also explored, it was calculated using the following mathematical formulations [9,10] :

$$\lambda = \frac{l_m \sqrt{12}}{t_w} \quad (6)$$

$$l_m = 0.5\sqrt{S^2 - {d_0}^2} \, . \quad (7)$$

The Discussion of results will be in terms of: ultimate load enhancement, load-vertical displacement response, failure mode and bond behavior.

Results and discussion

The results of the FE investigation are described in the next section, each specimen was given a name: the first character in each specimen designation is the name of the tested beam, followed by the CFRP stiffening configuration (PS1 or PS2), and finally the CFRP profile thickness. For example, "A2-PS1-3" is the cellular beam "A2" reinforced with bonded CFRP profiles of 3mm in one side of the vulnerable regions. It should also be noted that the discussion of results was separated into two groups according to dimensions and structural behavior of strengthened beams: Group 01 comprises specimen A2 and specimen B2 while Group 2 includes specimens A5 and B5.

T section strengthening

The load-deflection cves of all FRP T section strengthened beams are plotted in Figs. 14 and 15. Tab. 5 lists the ultimate load capacities of stiffened and unstiffened cases. It can be seen that Group 1 strengthened specimens have demonstrated identical responses in all cases, this can clearly be shown in Fig. 14, despite the fact that they all had significantly higher strength than control beams (around 47 % for A2 strengthened beams and around 32 % for B2 strengthened beams), the use of different profile thicknesses and strengthening configurations did not produced the desired difference in load enhancement, and the reached ultimate loads were close in all cases. On the other hand, the percentage of ultimate load augmentation for Group 2 reinforced beams varied depending on the strengthening technique and the T section profile thickness (Tab. 5) when compared to control beams A5 and B5, the strength gain ranged from 24% to 38% and 16% to 31 %, respectively. The ultimate load improved as the profile thickness increased. For all Group 2 scenarios, the PS2 arrangement outperformed the PS1 configuration in terms of strength. Due to the identical structural behavior of Groupe 2 tested beams, the load-vertical displacement response of A5 and B5 reinforced beams were extremely comparable (Fig.15), the load curves for PS1 configuration with one side stiffening declined earlier than for PS2 configuration, indicating the earlier beam failure.

The bond behavior has been checked using the numerical output SDEG (stress degradation). For Group 1 tested beams debonding happened in all PS1 situations. However, the SDEG value did not approach 1 in any PS2 configuration (Tab. 6). This was explained by the complement of adhesive layers facing each other's resistance [19]**.** It can also be noticed from Tab. 6 that brittle debonding occurred in all cases of Group 2 beams, which might be explained by the sudden buckling of the slender web post. Therefore, regarding the bond behavior and the web post slenderness in all cases of strengthened beams, debonding was primarily influenced by the web post slenderness. Different failure mode of Group 1 tested beams was observed. For A2 strengthened beams, the failure mode was changed to Vierendeel failure with slight debonding of T section profile for PS1 configuration (Fig.16). Although web post-buckling was not avoided for B2-PS1-3 and B2-PS1-6 (Fig.17), a profile thickness of 10 mm (B2-PS1-10) was willing to alter the stress state of the beam and change the failure mode to Vierendeel failure, which was also accompanied by slight profile debonding. As previously stated, the PS2 arrangement allowed the tested beams to fail via vierendeel failure without debonding, confirming that using CFRP on both sides of the web post helps to prevent the bond separation failure mode. In contrast to the aforementioned Group 1 beams, all Group 2 strengthened beams failed by T section debonding due to an excessive web post-buckling (Fig. 18), indicating that, unlike the aforementioned Group 1 beams, the pultruded T section stiffeners were unable to change the failure modes of Group 2 strengthened beams, the undesirable web post-buckling was only delayed to a higher load.

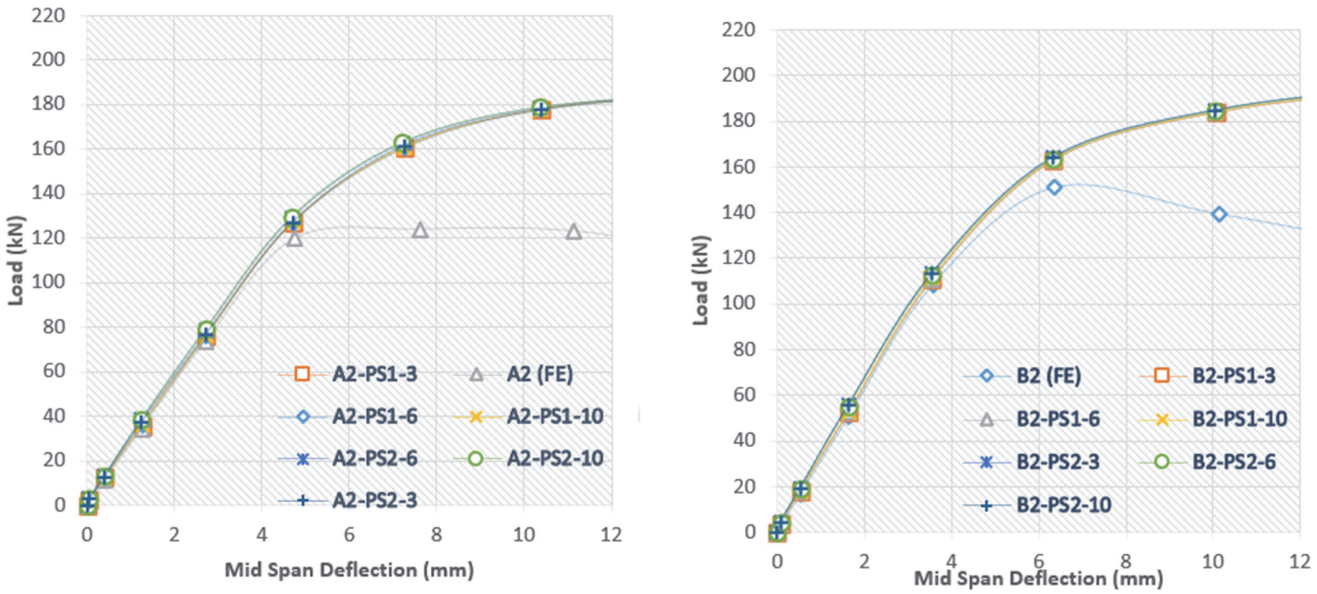

Figure 14: Load -deflection curves of Groupe 1 tested specimens.

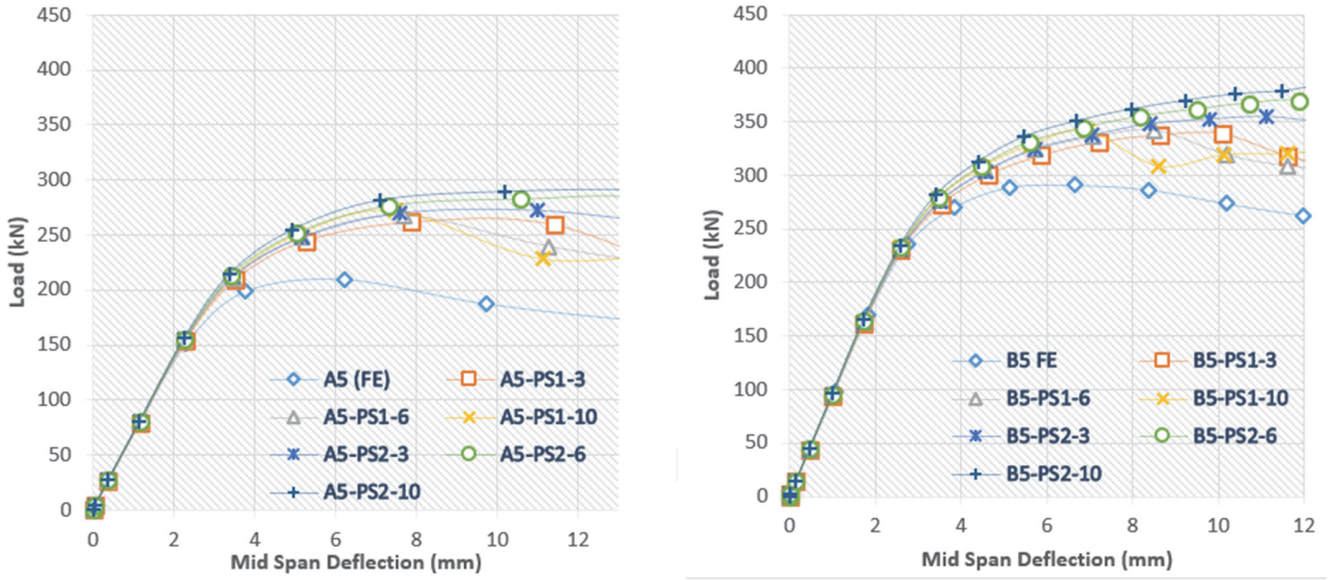

Figure 15: Load -deflection curves of Groupe 2 tested specimens.

U section strengthening

As mentioned before with the T section profile, the strength improvement employing the U profile section for Groupe 1 reinforced beams was roughly 47 percent and 32 percent for all cases of A2 and B2 strengthened beams, respectively (Tab. 7), The load level was the same as with the T section profile, but the U section shape had a slightly greater percentage of augmentation. Besides to that, the load-vertical displacement response for A2 and B2 strengthened beams was similar, and the strengthening technique and increased profile thickness had no effect on the strength enhancement (Fig.19). Moreover, compared to the T section strengthening, very interesting results were achieved using the U section carbon profile to strength A5 and B5 specimens. According to the strengthening technique and U profile thickness, Group 2 strengthened beams showed an increase ranged from 26% to 39% and 20% to 34% for A5 and B5 respectively (Tab. 7), (Fig. 20), confirming that the additional strength and stiffness were based on the pultruded stiffener geometry which relies on the moment of inertia of the pultruded section for the out of plane resistance [19]. It should also be mentioned that the load-displacement curves of PS1 configuration dropped sooner than PS2 configuration for Group 2 tested beams.

Specimen	P_u (kN)	Strength enhancement (%)
A2	123.82	/
A2-PS1-3	182.58	47.45
A2-PS1-6	182.63	47.49
A2-PS1-10	182.67	47.52
A2-PS2-3	182.82	47.64
A2-PS2-6	183.12	47.89
A2-PS2-10	183.18	47.94
B2	151.18	/
B2-PS1-3	198.09	31.02
B2-PS1-6	199.00	31.22
B2-PS1-10	199.35	31.86
B2-PS2-3	199.58	32.01
B2-PS2-6	199.95	32.25
B2-PS2-10	200.29	32.48
A5	209.63	/
A5-PS1-3	261.71	24.84
A5-PS1-6	267.42	27.56
A5-PS1-10	272.11	29.80
A5-PS2-3	272.51	29.99
A5-PS2-6	282.59	34.80
A5-PS2-10	290.65	38.64
B5	290.77	/
B5-PS1-3	339.27	16.67
B5-PS1-6	342.31	17.72
B5-PS1-10	342.32	17.72
B5-PS2-3	354.61	21.95
B5-PS2-6	368.9	26.87
B5-PS2-10	381.75	31.28

Table 5: Ultimate load results.

Specimen	web post slenderness	SDEG	Failure mode
A2	102.84	/	WPB
A2-PS1-3	102.84	1	V+DEB
A2-PS1-6	102.84	1	V+DEB
A2-PS1-10	102.84	1	V+DEB
A2-PS2-3	102.84	0	V
A2-PS2-6	102.84	0	V
A2-PS2-10	102.84	0	V
B2	94.09	/	WPB
B2-PS1-3	94.09	1	WPB+DEB
B2-PS1-6	94.09	1	WPB+DEB
B2-PS1-10	94.09	1	V+DEB
B2-PS2-3	94.09	0	V
B2-PS2-6	94.09	0	V
B2-PS2-10	94.09	0	V
A5	75.50	/	WPB
A5-PS1-3	75.50	1	WPB+DEB
A5-PS1-6	75.50	1	WPB+DEB
A5-PS1-10	75.50	1	WPB+DEB
A5-PS2-3	75.50	1	WPB+DEB
A5-PS2-6	75.50	1	WPB+DEB
A5-PS2-10	75.50	1	WPB+DEB
B5	59.11	/	WPB
B5-PS1-3	59.11	1	WPB+DEB
B5-PS1-6	59.11	1	WPB+DEB
B5-PS1-10	59.11	1	WPB+DEB
B5-PS2-3	59.11	1	WPB+DEB
B5-PS2-6	59.11	1	WPB+DEB
B5-PS2-10	59.11	1	WPB+DEB

Table 6: Bond-behavior and failure mode.

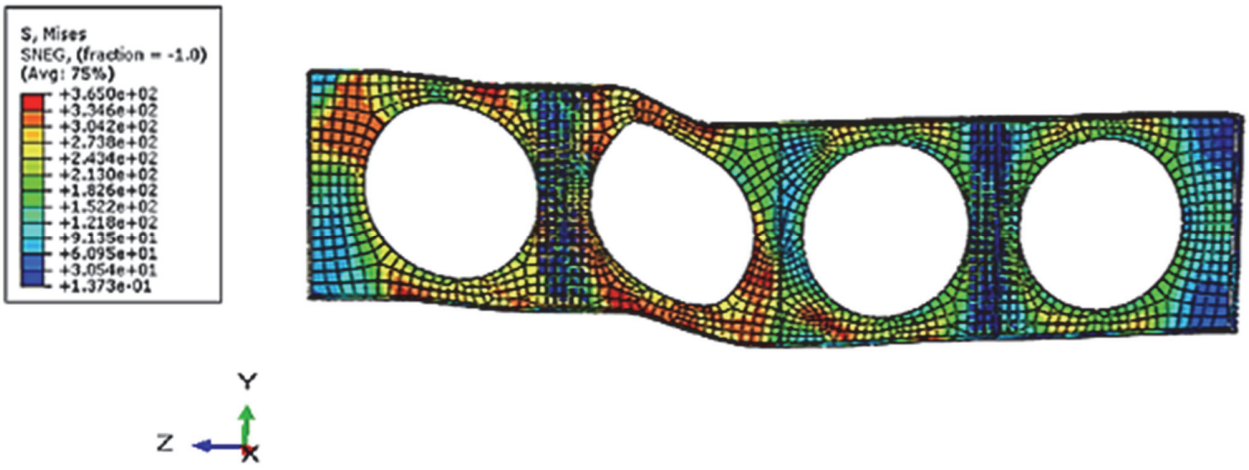

Figure 16: Vierendeel failure mode for specimen: B2 -PS2-3.

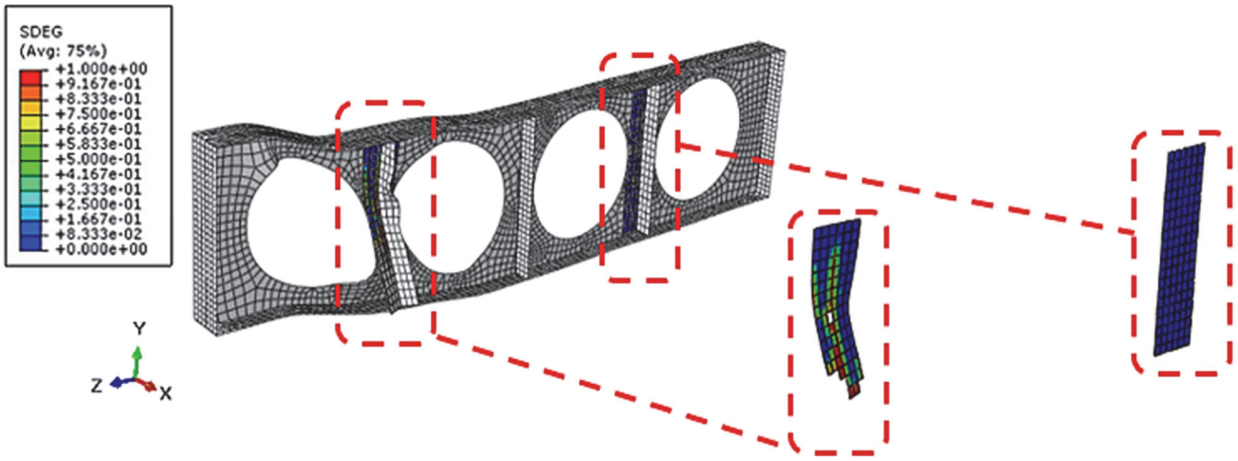

Figure 17: Checking bond behavior using SDEG parameter and adhesive layer deletion for specimen: B2 -PS1-3.

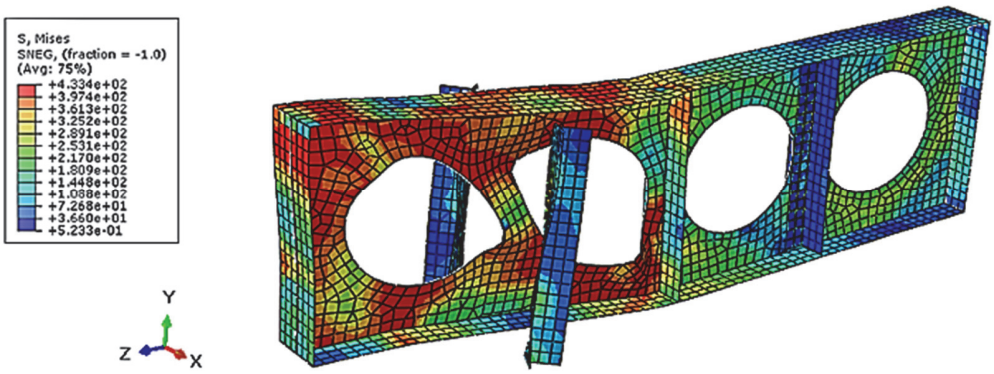

Figure 18: Web post-buckling failure mode and profile debonding for specimen: A5-PS2-6.

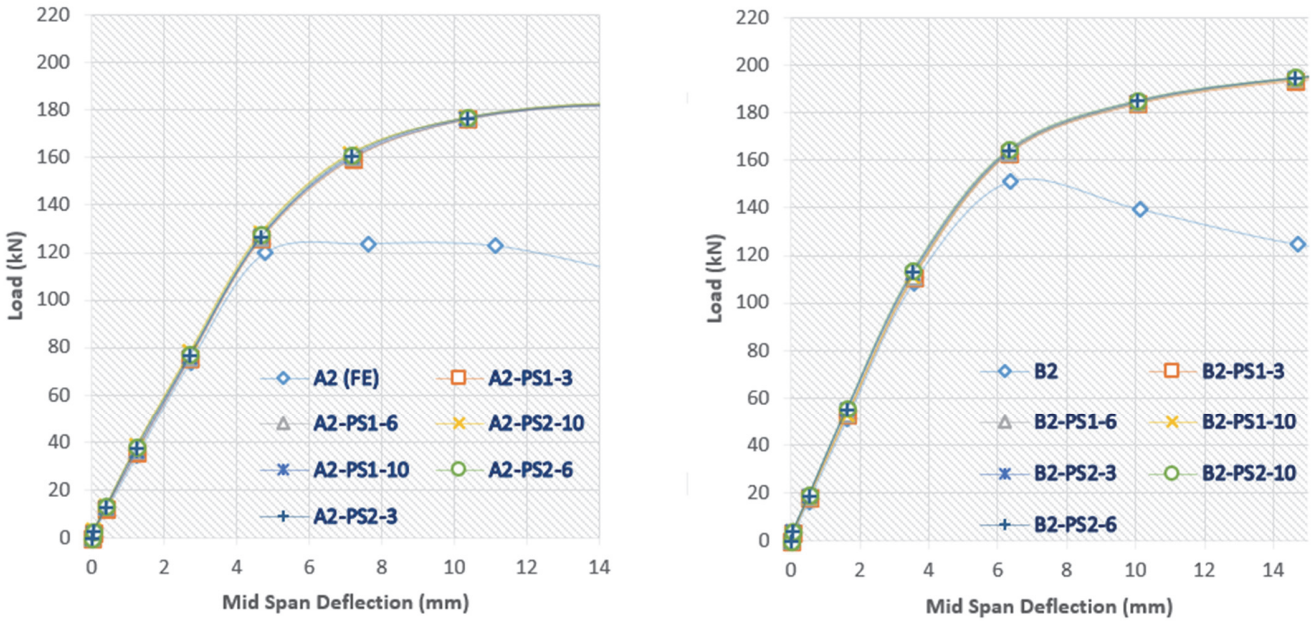

Figure 19: Load -deflection curves of Groupe 1 tested specimens.

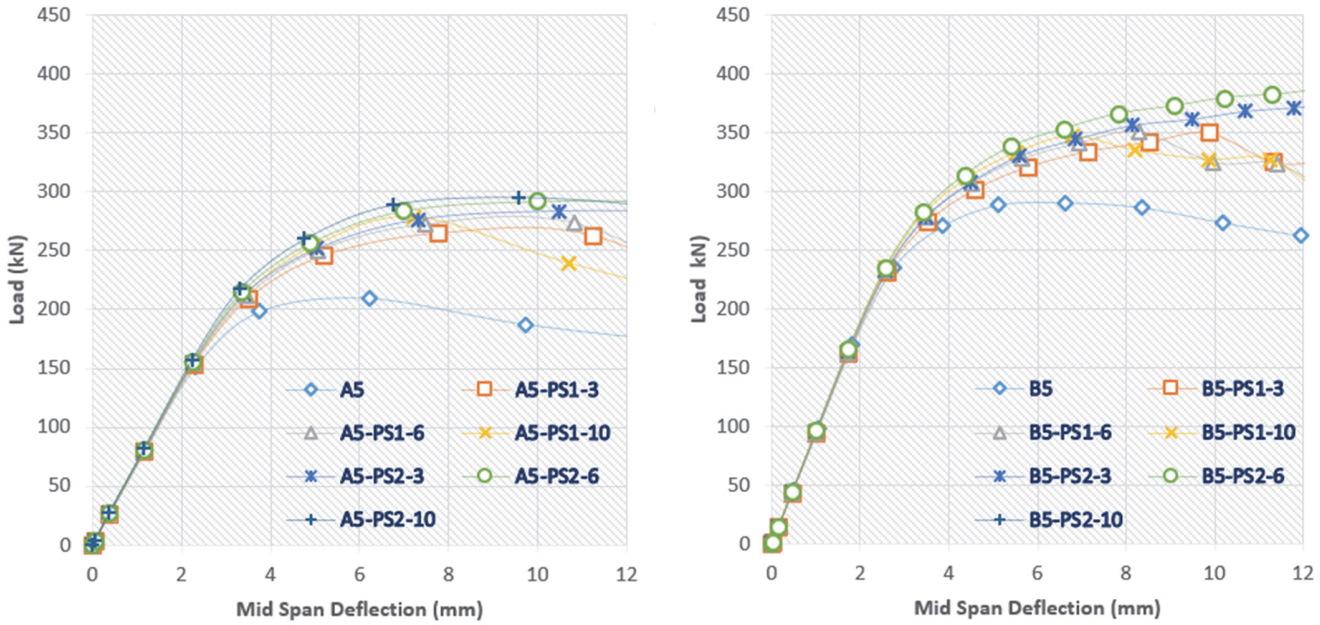

Figure 20: Load -deflection curves of Groupe 2 tested specimens.

Bond behavior of Group 1 and Group 2 strengthened beams adopting U carbon PFRP was similar to T section strengthening. Debonding occurred for PS1 configuration of Group 1 strengthened beams (Fig. 21) and all Group 2 strengthened beams (Tab.8). It was observed that the failure mode was also similar to T section strengthening (Fig. 21) only B2-PS1-6 which failed by Vierendeel failure mode and A5-PS2-10 which failed by top flange buckling which was followed by a slight debonding, indicating that stress concentration and failure mode had shifted away from the reinforced zone. Therefore, for both profile shapes, the PS2 configuration was the most effective technique in all circumstances, with 3 mm profile thickness for group 1 and 10 mm profile thickness for group 2.

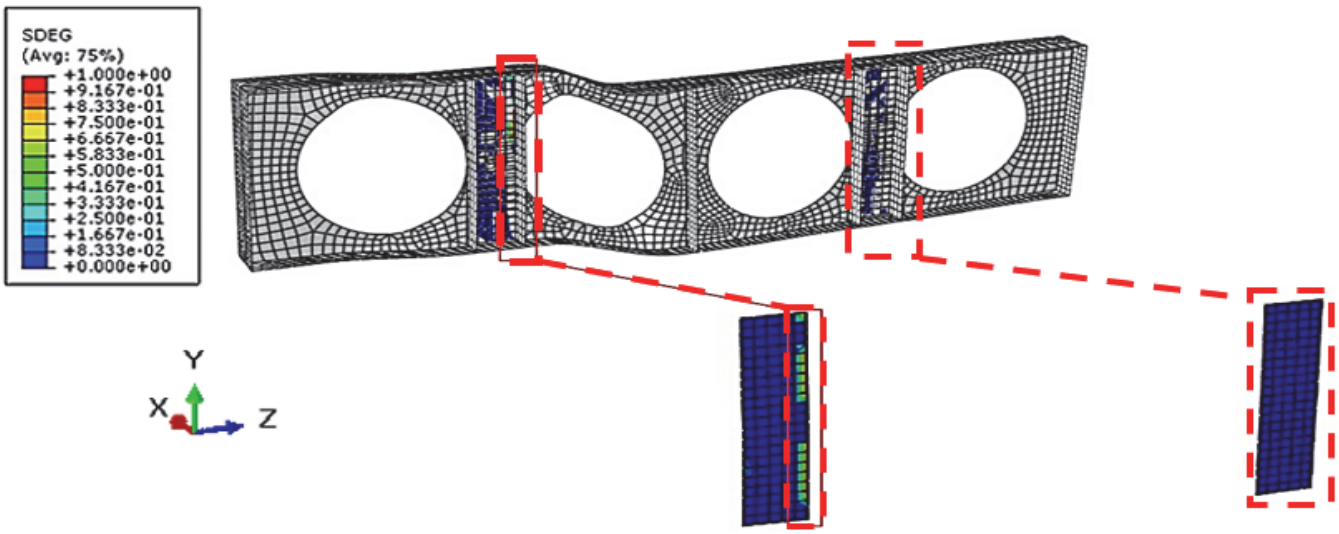

Figure 21: Bond behavior for specimen B2 -PS1-6.

Specimen	P_u (kN)	Strength enhancement (%)
A2	123.82	/
A2-PS1-3	182.67	47.52
A2-PS1-6	182.72	47.56
A2-PS1-10	182.79	47.62
A2-PS2-3	182.96	47.76
A2-PS2-6	183.16	47.92
A2-PS2-10	183.24	47.98
B2	151.18	/
B2-PS1-3	198.88	31.55
B2-PS1-6	199.24	31.78
B2-PS1-10	199.58	32.01
B2-PS2-3	199.96	32.26
B2-PS2-6	200.27	32.47
B2-PS2-10	200.38	32.54
A5	209.63	/
A5-PS1-3	265.19	26.50
A5-PS1-6	273.22	30.33
A5-PS1-10	278.62	32.91
A5-PS2-3	283.61	35.29
A5-PS2-6	292.17	39.37
A5-PS2-10	292.55	39.55
B5	290.77	/
B5-PS1-3	350.43	20.51
B5-PS1-6	350.85	20.66
B5-PS1-10	350.88	20.67
B5-PS2-3	376.57	29.50
B5-PS2-6	389.22	33.85
B5-PS2-10	391.26	34.55

Table 7: U section ultimate load results

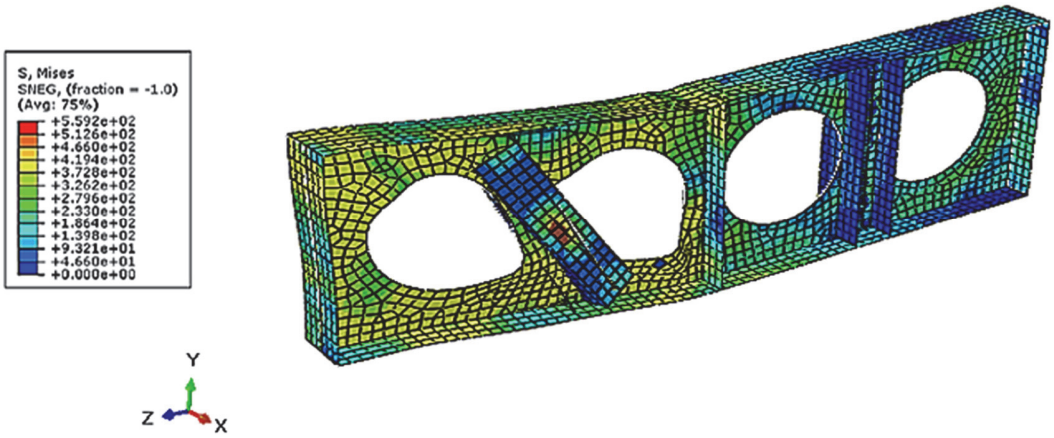

Figure 22 : Spécimen B2 -PS1-6 Failure mode.

Specimen	web post slenderness	SDEG	Failure mode
A2	102.84	/	WPB
A2-PS1-3	102.84	1	V+DEB
A2-PS1-6	102.84	1	V+DEB
A2-PS1-10	102.84	1	V+DEB
A2-PS2-3	102.84	0	V
A2-PS2-6	102.84	0	V
A2-PS2-10	102.84	0	V
B2	94.09	/	WPB
B2-PS1-3	94.09	1	WPB+DEB
B2-PS1-6	94.09	1	V+DEB
B2-PS1-10	94.09	1	V+DEB
B2-PS2-3	94.09	0	V
B2-PS2-6	94.09	0	V
B2-PS2-10	94.09	0	V
A5	75.50	/	WPB
A5-PS1-3	75.50	1	WPB+DEB
A5-PS1-6	75.50	1	WPB+DEB
A5-PS1-10	75.50	1	WPB+DEB
A5-PS2-3	75.50	1	WPB+DEB
A5-PS2-6	75.50	1	WPB+DEB
A5-PS2-10	75.50	1	TFY+DEB
B5	59.11	/	WPB
B5-PS1-3	59.11	1	WPB+DEB
B5-PS1-6	59.11	1	WPB+DEB
B5-PS1-10	59.11	1	WPB+DEB
B5-PS2-3	59.11	1	WPB+DEB
B5-PS2-6	59.11	1	WPB+DEB
B5-PS2-10	59.11	1	WPB+DEB

Table 8: Bond behavior and failure mode.

CONCLUSIONS

The goal of this study was to discover a new practical strengthening method for web post-buckling failure mode in cellular beams using the most effective CFRP profile section form and configuration. It was concluded that:

- Depending on the slenderness of the web post, this strengthening approach was able to avoid or delay web post-buckling to greater load in all situations.
- The effectiveness of this approach is largely dependent on the strengthening configuration and geometric properties of the CFRP profile, which offer an additional bending resistance to the web post.
- The use of bonded stiffeners on one side of web posts causes the earlier debonding of CFRP profiles
- Debonding CFRP profiles has a significant influence on strength enhancement, especially for slender web posts.
- The U section profile's superior performance can be attributed to its flexural stiffness, which is an order of magnitude more than that of the CFRP T section profile.
- The proposed strengthening technique improved the beam stiffness, web post yielding, and web post-buckling capacity.
- This study presents a primary investigation on the ability of CFRP profiles to strengthen web post-buckling of cellular beams, further studies are in need as part on the ongoing research in this topic.

NOMENCLATURE

PFRP: Pultruded fiber reinforced polymer.
CFRP: Carbon fiber reinforced polymer.
GFRP: Glass fiber reinforced polymer.
h: Height of profile.
b_f : Width of flange.
t_f : Thickness of flange.
t_w : Thickness of web.
d_w : Height of web.
d_0 : Web opening diameter.
S_0 : Web post width.
S : Opening diameter and web post width
L: Length of the beam.
f_y : The yield strength of steel.
E: Young's modulus.
t_n , t_s and t_t : Peak values of the nominal stress.
∂_{max} : Tensile strength of the adhesive.
τ_{max} : Shear strength of the adhesive.
D : The scalar damage variable.
δ_m^{max} : The maximum effective relative displacement attained during the loading history.
$\delta_m^0 and \ \delta_m^f$: The effective relative displacement at the initiation and end of failure respectively.
λ: Web post slenderness.
l_m : The strut length.
P_u : Ultimate load.
SDEG : Stress degradation parameter.
WPB : Web post-buckling failure mode.
V: Vierendeel failure mode.
DEB: CFRP profile debonding.
TFY: Top flange yielding.
LTB: Lateral torsional buckling.

REFERENCES

[1] Zaarour, W., Redwood, R. (1996). Web Buckling in Thin Webbed Castellated Beams, J. Struct. Eng., 122(8), pp. 860–866, DOI: 10.1061/(ASCE)0733-9445(1996)122:8(860).
[2] Redwood, R., Demirdjian, S. (1998). Castellated Beam Web Buckling in Shear, J. Struct. Eng., 124(10), pp. 1202–1207, DOI: 10.1061/(ASCE)0733-9445(1998)124:10(1202).
[3] Galambos, A.R., Hosain, M.U., Speirs, W.G. (1975). Optimum expansion ratio of castellated steel beams, Eng. Optim., 1(4), pp. 213–225, DOI: 10.1080/03052157508960588.
[4] Kerdal, D., Nethercot, D.A. (1984). Failure modes for castellated beams, J. Constr. Steel Res., 4(4), pp. 295–315, DOI: 10.1016/0143-974X(84)90004-X.
[5] Silva, C.C., Caldas, R.B., Fakury, R.H., Carvalho, H., Dias, J.V.F. (2019). Web Rotational Stiffness of Continuous Steel-Concrete Composite Castellated Beams, Frat. Ed Integrità Strutt., 13(50), pp. 264–275, DOI: 10.3221/IGF-ESIS.50.22.
[6] Morkhade, S.G., Gupta, L.M. (2015). An experimental and parametric study on steel beams with web openings, Int. J. Adv. Struct. Eng., 7(3), pp. 249–260, DOI: 10.1007/s40091-015-0095-4.
[7] Morkhade, S.G., Gupta, L.M. (2019). Ultimate load behaviour of steel beams with web openings, Aust. J. Struct. Eng.,

20(2), pp. 124–133, DOI: 10.1080/13287982.2019.1607448.
[8] Tsavdaridis, K.D., D'Mello, C. (2011). Web buckling study of the behaviour and strength of perforated steel beams with different novel web opening shapes, J. Constr. Steel Res., 67(10), pp. 1605–1620, DOI: 10.1016/j.jcsr.2011.04.004.
[9] Panedpojaman, P., Thepchatri, T., Limkatanyu, S. (2014). Novel design equations for shear strength of local web-post buckling in cellular beams, Thin-Walled Struct., 76, pp. 92–104, DOI: 10.1016/j.tws.2013.11.007.
[10] Grilo, L.F., Fakury, R.H., Castro e Silva, A.L.R. de., Veríssimo, G. de S. (2018). Design procedure for the web-post buckling of steel cellular beams, J. Constr. Steel Res., 148, pp. 525–541, DOI: 10.1016/j.jcsr.2018.06.020.
[11] Darwin, D. (2003). Steel Design Guide Series Steel and Composite Beams with Web Openings Design of Steel and Composite Beams with Web Openings .
[12] (N.d.). Design of Composite Beams with Large weB openings, .
[13] Al-Thabhawee, H., Ali, H.W., Muhammed, A.H. (2019). The Effect Of Strengthening By Using Steel Ring Stiffeners On The Behavior Of The Cellular Beams With Large Web-Opening, Int. J. Sci. Technol. Res., 8, pp. 7, DOI: 10.13140/RG.2.2.24843.23848.
[14] Morkhade, S.G., Lokhande, R.S., Gund, U.D., Divate, A.B., Deosarkar, S.S., Chavan, M.U. (2020). Structural behaviour of castellated steel beams with reinforced web openings, Asian J. Civ. Eng., 21(6), pp. 1067–1678, DOI: 10.1007/s42107-020-00262-y.
[15] Zhao, X.L., Al-Mahaidi, R. (2009). Web buckling of lightsteel beams strengthened with CFRP subjected to end-bearing forces, Thin-Walled Struct., 47(10), pp. 1029–1236, DOI: 10.1016/j.tws.2008.10.009.
[16] Narmashiri, K., Ramli Sulong, N.H., Jumaat, M.Z. (2011). Flexural strengthening of steel I-beams by using CFRP strips, Int. J. Phys. Sci., 6(7), pp. 1620–1627, DOI: 10.5897/IJPS11.140.
[17] Zeng, J.-J., Gao, W.-Y., Liu, F. (2018). Interfacial behavior and debonding failures of full-scale CFRP-strengthened H-section steel beams, Compos. Struct., 201, pp. 540–552, DOI: 10.1016/j.compstruct.2018.06.045.
[18] Okeil, A.M., Bingol, Y., Ferdous, M.R. (2009). Novel Technique for Inhibiting Buckling of Thin-Walled Steel Structures Using Pultruded Glass FRP Sections, J. Compos. Constr., 13(6), pp. 547–557, DOI: 10.1061/(ASCE)CC.1943-5614.0000034.
[19] Ulger, T., A.M. Okeil. (2016). LSU Digital Commons Strengthening Shear Deficient Thin-Walled Steel Beams by Bonding Pultruded GFRP Sections.
[20] Altaee, M.J., Cunningham, L.S., Gillie, M. (2017). Experimental investigation of CFRP-strengthened steel beams with web openings, J. Constr. Steel Res., 138, pp. 750–760, DOI: 10.1016/j.jcsr.2017.08.023.
[21] Altaee, M., Cunningham, L.S., Gillie, M. (2019). Practical Application of CFRP Strengthening to Steel Floor Beams with Web Openings: A numerical Investigation, J. Constr. Steel Res., 155, pp. 395–408, DOI: 10.1016/j.jcsr.2019.01.006.
[22] Mustafa, S.A., Fathy, E., Rizk, M.S. (2020). Fiber-reinforced polymer plates for strengthening web opening in steel I-beams under cyclic loading, Adv. Struct. Eng., 23(2), pp. 348–359, DOI: 10.1177/1369433219868073.
[23] Hamood, M., Abdulsahib, W., Abdullah, A. (2018).The effectiveness of CFRP strengthening of steel plate girders with web opening subjected to shear. MATEC Web of Conferences, 162, EDP Sciences.
[24] Cyril Thomas, A., Baskar, K. (2018). Strengthening of thin-webbed castellated beam using CFRP, Int. J. Comput. Methods Eng. Sci. Mech., 19(6), pp. 396–404, DOI: 10.1080/15502287.2018.1534153.
[25] Farid, B., Boutagouga, D. (2021). Parametric study of I-shaped shear connectors with different orientations in push-out test, Frat. Ed Integrità Strutt., 15(57), pp. 24–39, DOI: 10.3221/IGF-ESIS.57.03.
[26] Namdar, A., Dong, Y., Liu, Y. (2018). Timber beam seismic design – A numerical simulation, Frat. Ed Integrità Strutt., 13(47), pp. 451–458, DOI: 10.3221/IGF-ESIS.47.35.
[27] Jafari, F., Badarloo, B. (2019). Finite Element Analysis and ANFIS investigation of seismic behavior of sandwich panels with different concrete material in two story steel building, Frat. Ed Integrità Strutt., 13(50), pp. 209–230, DOI: 10.3221/IGF-ESIS.50.18.
[28] Dar, M.A., Subramanian, N., Dar, A.R., Anbarasu, M., Lim, J.B., Atif, M. (2019). Behaviour of partly stiffened cold-formed steel built-up beams: Experimental investigation and numerical validation, Adv. Struct. Eng., 22(1), pp. 172–186, DOI: 10.1177/1369433218782767.
[29] (N.d.). ABAQUS, 2013. Theory Manual, User Manual and Example Manual Version 6., Dassault Systemes Simulia Corp.
[30] Swinnen, J. (n.d.). Modelling FRP open-hole tensile tests in Abaqus, .
[31] Bennati, S., Colonna, D., Valvo, P.S. (2016). Evaluation of the increased load bearing capacity of steel beams strengthened with pre-stressed FRP laminates, Frat. Ed Integrita Strutt., 10(38), pp. 377–391, OI: 10.3221/IGF-ESIS.38.47.